

IET Microwaves, Antennas & propagation

Special issue Call for Papers



Be Seen. Be Cited.
Submit your work to a new
IET special issue

"Green antenna
technologies enabling
sustainable RFID and IoT
systems"

Guest Editors: Riccardo
Colella, Almudena
Rivadeneira, Massimo
Merenda and Antonio Alex-
Amor



[Read more](#)



The Institution of
Engineering and Technology

ORIGINAL RESEARCH

Electromagnetic characterisation of conductive 3D-Printable filaments for designing fully 3D-Printed antennas

Riccardo Colella¹ | Francesco Paolo Chietera¹ | Andrea Michel²  | Giacomo Muntoni³ | GiovanniAndrea Casula³ | Giorgio Montisci³ | Luca Catarinucci¹ 

¹Department of Innovation Engineering, University of Salento, Lecce, Italy

²Department of Information Engineering, University of Pisa, Pisa, Italy

³Dipartimento di Ingegneria Elettrica ed Elettronica, University of Cagliari, Cagliari, Italy

Correspondence

Andrea Michel, Department of Information Engineering, University of Pisa, Via G. Caruso, 16, Pisa 56122, Italy.
Email: andrea.michel@unipi.it

Funding information

Fondazione di Sardegna, Grant/Award Number: F74I19001060007

Abstract

Additive manufacturing (AM) 3D-printing technology is increasingly bringing benefits even in electromagnetics, with interesting prospects of application. Apart from the use of additive manufacturing for realising dielectric components of suitably shaped antennas, the ambitious target is, undoubtedly, the fully 3D realisation of radiofrequency and microwave circuits as well as radiating structures, including, therefore, conductive parts. In this regard, 3D-printable filaments with interesting conductive properties are being produced. However, their rigorous conductivity characterisation is still missing, making it difficult to estimate the real behaviour of the final 3D printed electromagnetic device. To fill this gap, the conductivity of one of the most interesting conductive filaments, named Electrifi, is first experimentally evaluated in a frequency range as large as 0.72–6 GHz, accounting also for its roughness. Then it has been validated by designing, realising, and testing three fully 3D-printed antennas. Specifically, two bow-tie antennas, operating at 2.8 and 4 GHz, respectively, and an ultrawideband antenna, borrowed from the existing literature, operating between 1 and 7 GHz. The good agreement between simulated and measured results demonstrates the reliability of the performed electrical conductivity characterisation, even in the design of efficient radiating structures entirely realised with thermoplastic materials with copper nanoparticle additives.

1 | INTRODUCTION

Additive Manufacturing (AM) by 3D printing is undergoing a considerable technological advancement in the scientific field and its qualities can be highly valuable even for the antenna designers since they involve easy fabrication and low-cost production. The fabrication of highly detailed and complicated antenna layouts could be carried out by exploiting these new AM technologies, including laser powder bed fusion, binder jetting, vat photopolymerisation, material jetting, direct energy deposition, sheet lamination, and fused filament fabrication (FFF) [1, 2]. Among them, FFF is particularly suitable thanks to its cost-effectiveness and ease of use. However, the scientific community is struggling to provide effective and reliable design of cost-effective fully 3D-printed antennas. Indeed, the 3D-printed metallisation over thermoplastic substrates is still a challenging task, typically faced either by using

expensive 3D metal printers [1] or by using the binder jetting technique [3].

For these reasons, in the open literature, 3D printing based on material extrusion is mainly employed to build only the dielectric structure of the antenna, falling back on alternative solutions to provide the metallisation [4–27]. Many types of antennas operating at very different frequencies and many techniques to realize the conductive parts have been adopted in these works. The most meaningful ones are described below. In Ref. [4], Colella *et al.* proposed a 3D-printed circularly polarised antenna for Radiofrequency Identification applications, using a polylactic acid (PLA) substrate, and adding conductive tape to provide the metallisation. However, conductive tape cutting requires high precision, particularly for high frequencies, and must be performed using reliable techniques. In Ref. [5], Mirzozafari *et al.* relied on 3D-printing for the supporting structure of an array of dipoles, but the metallisation was provided by

This is an open access article under the terms of the Creative Commons Attribution-NonCommercial License, which permits use, distribution and reproduction in any medium, provided the original work is properly cited and is not used for commercial purposes.

© 2022 The Authors. *IET Microwaves, Antennas & Propagation* published by John Wiley & Sons Ltd on behalf of The Institution of Engineering and Technology.

means of electroplating. Other efforts have been made by employing conductive ink [6], or spray coating [7], but conductive ink needs dedicated curing processes, whereas spray coating does not easily offer a homogeneous distribution. Furthermore, each of the aforementioned solutions is characterised by a double step in the fabrication process: one step devoted to the assembling of the supporting and/or dielectric medium and one step for the conductive counterpart. This adds complexity to the manufacturing process and contextually increases the overall production cost. Ideally, since the antenna designer must deal with the imperfections of the thermoplastic materials, a unique process using a dual extruder printer would be preferable.

In this context, the availability of conductive filaments for 3D printers could actually pave the way to 3D-printing in electromagnetics. Some filaments are on the market. They are composed of a blend of polymers and a certain percentage of conductive parts: carbon nanotubes in the Fiberforce Conductive filament [28], conductive black carbon in the Proto-Pasta filament [29], graphene in the Black-Magic filament [30], or even copper, as in the case of the Electrifi filament [31] produced by Multi3D (Cary, North Carolina, USA). From preliminary tests, Electrifi appears to be the most promising one, and some works exploiting its properties to realise 3D-printed antennas and microwave devices are already published, [2, 32–37]. In particular, in Ref. [32], a simple microstrip transmission line printed on a 62 mil Rogers TMM4 substrate by using the Electrifi filament has been analysed, concluding that it might represent an alternative to the regular copper transmission line at least for applications up to 3 GHz. The maximum frequency of 3 GHz has been then extended to 5 GHz in Ref. [33]. Fully 3D-printed antennas have been also presented in Refs. [2, 34], based on Electrifi and PLA. Specifically, in Ref. [34], the comparison between the losses of a standard transmission line, etched on FR4, and one made with PLA and Electrifi has been carried out up to 10 GHz, by also varying the infill percentage and infill pattern parameters. However, until now Electrifi-based antennas have been mainly simulated using a constant value of conductivity, typically of 16,000 S/m, provided by the manufacturer [31], and this may represent a non-negligible approximation during wideband antenna and circuit design.

Whilst the electrical performance of different dielectric filaments is available in the literature (e.g. in Ref. [37]), only few papers have been devoted to the electromagnetic characterisation of Electrifi over a wide frequency range. For example, in Ref. [35], the attenuation and phase constant from the measured reflection and transmission coefficients have been estimated up to 4 GHz by using a 50 Ω Electrifi transmission line. In Ref. [36], a wideband assessment of the transmission losses of 3D-printed waveguides that use the Electrifi filament for manufacturing has been presented by analysing four standard waveguides in the frequency band of 8–40 GHz. In addition to the aforementioned remarkable results, a further characterisation of Electrifi—for instance, in terms of conductivity over the frequency—would be relevant from the scientific and applicative point of view.

In this work, an electromagnetic characterisation in terms of conductivity of the Multi3D Electrifi filament has been performed in a wide frequency range (0.72–6 GHz) by using a set of specifically designed 3D-printed resonators. In view of the use of Electrifi in fully 3D electromagnetic devices, such characterisation accounts for all the related effects, including the potential deposition of the conductive polymer on a printed PLA substrate, opportunely characterised as well, and the surface roughness of both substrate and conductive parts. The conductivity estimation is definitely found by fitting experimental results with those obtained with a numerical model.

Finally, to validate the performed Electrifi characterisation, two fully 3D-Printed bow-tie antennas resonating at 2.8 and 4 GHz, respectively, as well as a wideband antenna [38] covering almost the entire frequency band under consideration have been designed, manufactured and tested. The good adherence between measurements and simulations, both in terms of return loss and radiation patterns, validated the electrical conductivity characterisation performed and confirmed that Electrifi is a suitable material to design 3D-printed antennas up to 6 GHz.

2 | CHARACTERISATION OF THE THERMOPLASTICS

The thermoplastic 3D-printable materials used in this work are a standard PLA, for the realisation of dielectric structures, and the Multi3D Electrifi, for the realisation of 3D-printed conductive parts. To evaluate the electromagnetic properties of the realised structures, the possible impact of the surface roughness has been preliminarily assessed. Indeed, it is worth highlighting that when electromagnetic 3D-printed structures are considered, the surface roughness could affect the structure performance, especially when it is not sufficiently smaller than the skin depth [39–41]. For this reason, the roughness of two 3D-printed Electrifi and PLA samples has been verified with a Veeco Dektak 150 profilometer (see Figure 1a), equipped with a 12.5 nm stylus. The stylus has run across 1 cm of the sample surfaces, along the direction of maximum irregularity due to the Fused Deposition Modeling printing pattern. In Figure 1b, the measured roughness profiles of both the PLA and Electrifi structures are plotted. The resulting root mean square (RMS) values are 13.33 and 12.82 μm for the Electrifi and PLA sample, respectively. With the aim of accurately reproducing all the 3D-printed structures designed in this work, such roughness values will be hereafter considered in the related numerical model used to perform the electromagnetic simulations.

A first analysis has been performed on the 3D-printed PLA material. The microstrip T-resonator method [42, 43] has been used to evaluate both the relative dielectric constant (ϵ_r) and loss tangent ($\tan\delta$) at some specific resonance frequencies. In particular, a microstrip T-resonator with a stub length of 65 mm and width of 3.8 mm has been designed with adhesive copper tape—instead of Electrifi, thus clearly distinguishing the sole PLA contribution at this stage—and applied on a 3D-printed PLA substrate of thickness 1.2 mm.

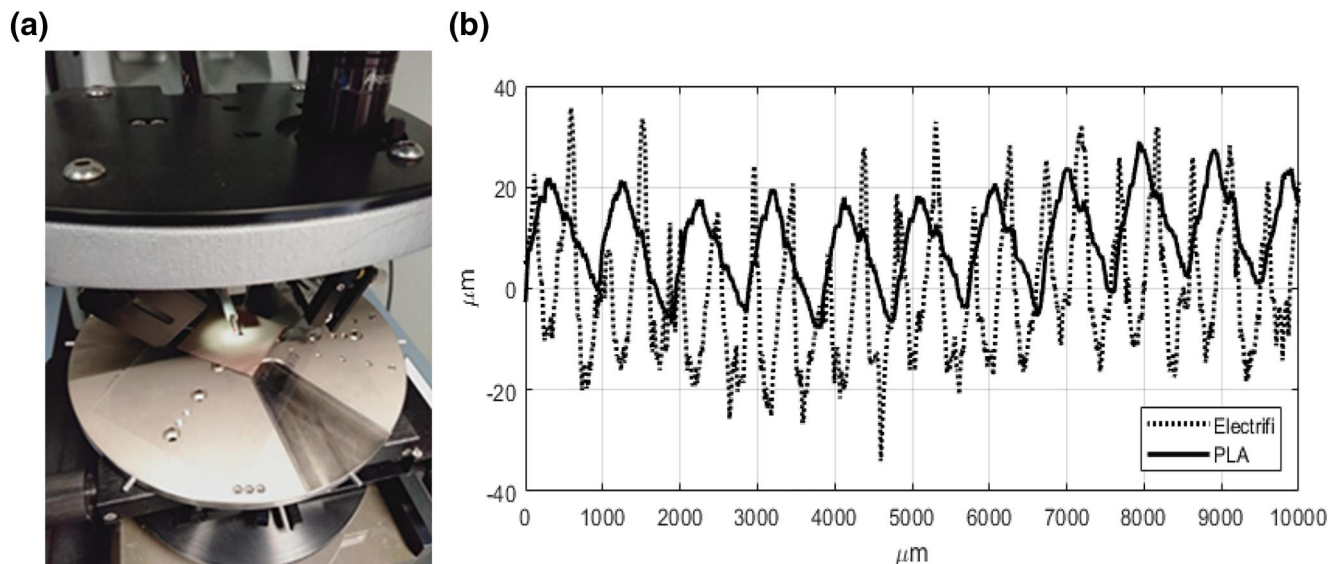


FIGURE 1 (a) Picture of the Veeco Dektak 150 profilometer and (b) electrifi (dotted) and polylactic acid (PLA) (solid) surface roughness profiles

With this configuration, a first resonance at 0.72 GHz has been obtained. Then, the stub length has been progressively reduced in steps of 2 mm so as to increase the resonance frequency.

For each stub length, the S_{21} scattering parameter has been measured by using an Agilent E5071C Vector Network Analyser (VNA) and then both ϵ_r and $\tan\delta$ have been indirectly obtained through known formulas [43] in the range 0.72–6.37 GHz. The VNA has been purposely calibrated by using the Short-Open-Load-Through (SOLT) method by setting the terminations of the two 50 Ω coaxial probes (i.e. the probes used to interface the VNA with T-Resonator ports) as calibration planes. In this way, the effect of the VNA probes is purposely de-embedded from the measurements. Polylactic acid characterisation at single frequencies is plotted in Figure 2 (circle markers) along with the related interpolation curve (continuous line). It can be observed that, as expected, due to the constant reduction step of the stub length, the distribution of measurement points does not vary linearly with the frequency, with a higher concentration of points at lower frequencies. While frequency increases, ϵ_r ranges from 2.75 to 2.40 (Figure 2a), and the loss tangent ranges from 0.007 to 0.025 (Figure 2b). To confirm the correctness of the PLA measurements, before introducing any Electrifi-made conductive parts, results have been firstly compared with those available in the literature and then with the first-order Debye analytical model. More specifically, the dot-dashed lines of the graphs in Figure 2 represent a portion of the wideband measurement performed on a homogeneous sample of bulk PLA (not 3D-printed) reported in Ref. [44], and the dashed lines are referred to the PLA first-order Debye model curve. It can be observed that all the curves exhibit a similar trend in the investigated frequency band. Nevertheless, there are expected differences, mostly in terms of loss tangent. Such differences demonstrate the need to characterise the PLA substrates when AM 3D-Printing is adopted. Indeed, extruded PLA differs from bulk PLA, for instance, in terms of encapsulated air during the process, printing setup, related roughness, and other mechanical

characteristics. To better highlight such a difference, measured bulk PLA values have been extracted from the literature [44] and plotted in Figure 2 as well. As can be observed, there is a perfect agreement between the Debye model and data extrapolated from the literature for the case of bulk PLA, whilst the extruded PLA differs in certain points. This comparison confirms the accuracy of the implemented bulk PLA Debye model, since obtained permittivity values result in a perfect overlapping with the permittivity values extracted from bulk PLA measurements. On the other hand, the same analysis confirms that a difference between extruded PLA and bulk PLA exists and is quantified. For this reason, permittivity values of extruded PLA are considered in this work to model the material in the electromagnetic simulator.

As previously stated, the evaluation of the dielectric properties of PLA is propaedeutic to the estimation of the conductivity (σ) of the Electrifi material, which is, in turn, a mandatory task to provide the RF designer with all the needed parameters to design fully 3D-printed radiofrequency structures. For this goal, a two-step approach has been performed. Firstly, a T-resonator identical to the previous one (configuration with $L = 65$ mm) has been realised by replacing the copper-tape microstrip line with a 3D-printed 0.4 mm-thick Electrifi microstrip line. The realised fully 3D-printed T-resonator (Figure 3) has been characterised in terms of scattering parameters through the VNA between 0.72 and 6 GHz, thus obtaining a S_{21} curve in a wide frequency range. It corresponds to the solid line of Figure 4a where the typical T-resonator resonance peaks are clearly visible. As for the adopted printing settings, they are conveniently summarised in Table 1 in terms of extruding temperature, printing speed, nozzle diameter and extrusion multiplier, for both PLA and Electrifi.

In the second step, the same T-resonator has been designed using Computer Simulation Technology (CST) Microwave Studio [45]. In particular, the PLA has been modelled as a linear interpolation of the performed and validated measurements of

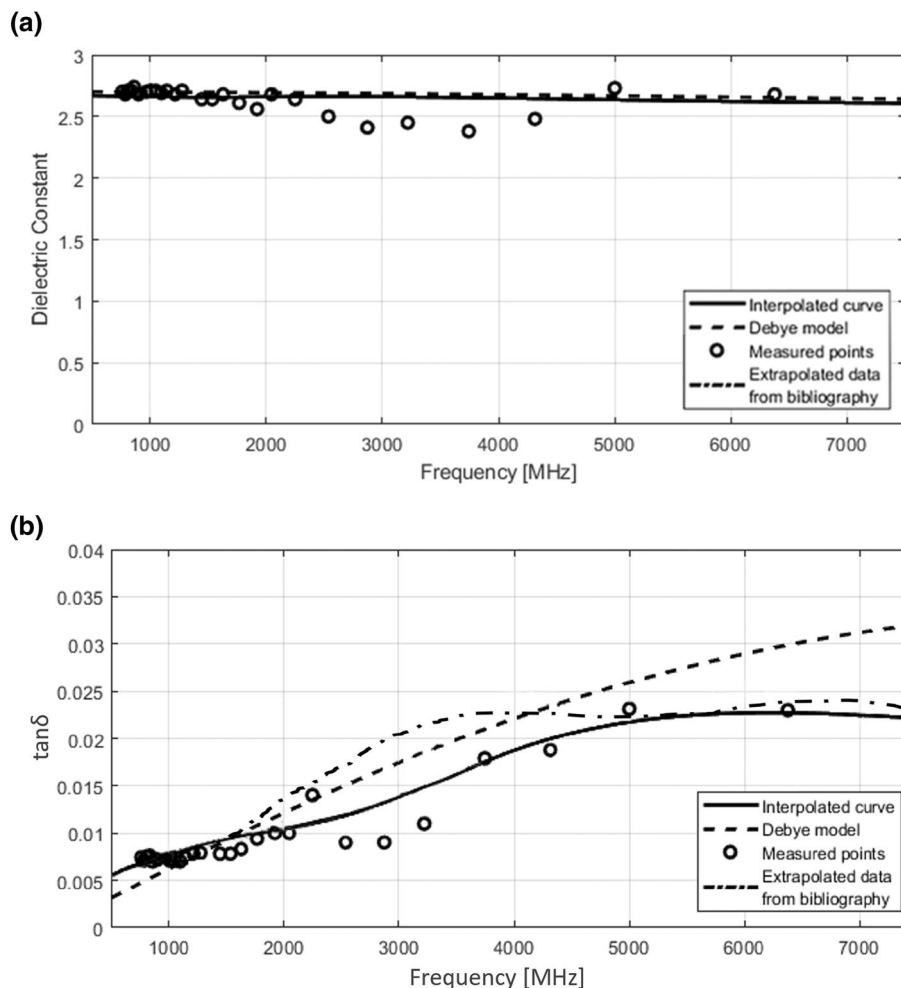


FIGURE 2 Dielectric constant (a) and loss tangent (b) values of the measured polylactic acid (PLA) over frequency



FIGURE 3 Picture of the fully 3D-printed T-resonator

ϵ_r and $\tan\delta$ (see Figure 2). The measured roughness of $12.82\ \mu\text{m}$ has been considered as well. Particular care has been dedicated to model the junction between the T-Resonator and external connectors. Both ports of the Electrifi-made microstrip structure have been electrically connected to a pair of Printed Circuit Boards (PCBs) Sub Miniature version A (SMA) connectors using an industrial silver epoxy (MG Chemicals 8331D) with a

cure time of 24 h at about 25°C . The conductivity of the used silver paste is $55\ \text{kS/m}$. As for the Electrifi modelling, a careful analysis is necessary. Specifically, the Electrifi has been modelled as a lossy metal with a density equal to $1.8\ \text{g/cm}^3$, a thermal conductivity of $1.5\ \text{W/mK}$ (values provided by the manufacturer), the measured RMS roughness of $13.33\ \mu\text{m}$, and an electrical conductivity σ , which is the unknown to be determined, purposely set as a variable parameter. Indeed, the manufacturer declared a conductivity value, which is around $16,000\ \text{S/m}$ [31], but no specific information about its value at radiofrequencies is provided. Several simulated S_{21} curves have been obtained by varying the parameter σ in steps $\Delta\sigma$ as low as $50\ \text{S/m}$. Each simulated curve has been then compared with the measured one, whose fitting level is, ultimately, the simulation target. The related RMS Error (RMSE) has been chosen as the fitting parameter. Consequently, it has been evaluated considering all the frequency points for all the simulated curves, starting from 0.72 to $6\ \text{GHz}$ in steps of $7\ \text{MHz}$.

At this regard, the curve minimising the RMSE resulted in an electrical conductivity $\sigma = 3400\ \text{S/m}$. For instance, the obtained Root Square Main Error has been as low as $0.61\ \text{dB}$, quite reduced considering that a relatively large frequency band has been accounted for. This result appears to be a better

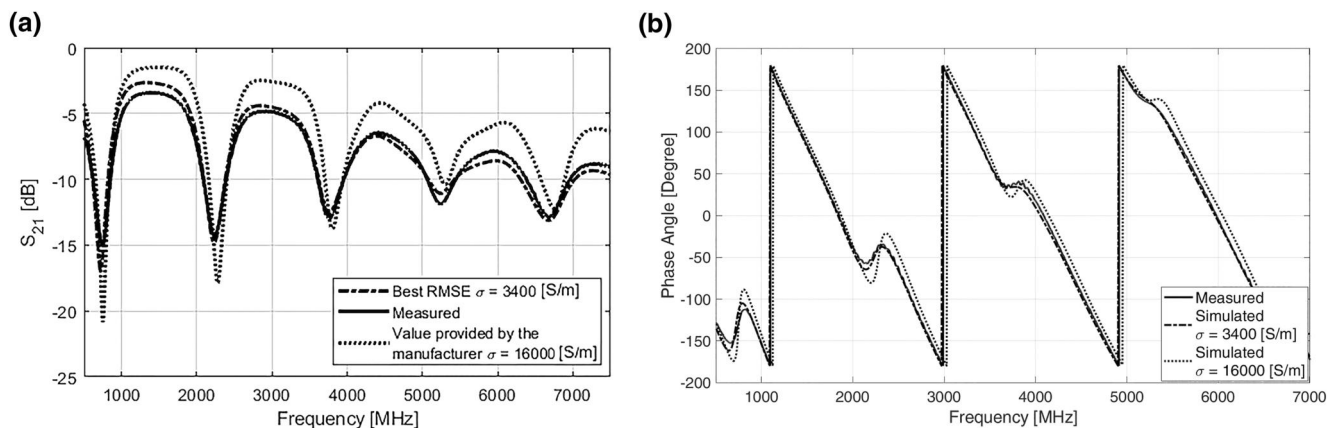


FIGURE 4 Comparison among the measured S₂₁ target curve (solid line), the simulated one with the value of electrical conductivity provided by the manufacturer (dotted line) and the one with the value that minimises the root mean square error (RMSE) on the whole analysed band (dot-dashed lines): module (a) and phase (b)

TABLE 1 Printing settings

Material	PLA	Electrifi
Extruding temperature	205°C	145°C
Printing bed temperature	60°C	25
Printing speed	2600 mm/min	600 mm/min
Nozzle diameter	0.5 mm	0.5 mm
Extrusion multiplier	100%	120%
Infill percentage	100%	100%
Layer height	0.2 mm	0.2 mm
Outline shells	3	1

approximation for the electrical conductivity of Electrifi with respect to that provided by the manufacturer (i.e. 16,000 S/m). Indeed, the latter produces a higher RMSE of 2.26 dB, as shown in Figure 4a, where a visual comparison between measured and simulated results is shown, both for $\sigma = 3400$ S/m and $\sigma = 16,000$ S/m. Finally, the same analysis has been reported in Figure 4b also in terms phase, and an optimal agreement between simulated and measured curves is obtained regardless of the adopted value for the conductivity.

A possible confirmation of the goodness of this lower value can be obtained by considering the results described in Ref. [34], where a 2.5 GHz patch antenna realised in Electrifi is discussed and prototyped. In that case, a non-perfect agreement between simulated and measured S₁₁ curves has been shown along with a gain lower than expected. Authors of Ref. [34], who used the conductivity declared by the manufacturer, justified the difference with the probable inaccuracy of the considered conductivity value and/or dielectric losses at radiofrequency. The analysis performed in the present work enforces the hypothesis theorised in Ref. [34] and, in addition, clarifies that the impact of dielectric losses is negligible when compared with the conductive ones, since the measured loss

tangent of PLA at 2.5 GHz is as low as 0.01 (half of those of FR4), whilst the drop in terms of conductivity is appreciable.

Despite the good agreement between the simulated curve considering $\sigma = 3400$ S/m and the measured one, it is clear from Figure 4 that in some frequency windows an even better match could be achieved. For this reason, since the RF designer is typically interested in narrower bands, the same analysis has been reiterated by evaluating the RMSE on four different frequency bands, slightly overlapped. In Table 2, the conductivity values obtained by minimising the RMSE in each considered band is reported, whilst the related comparison between measured and simulated curves for these values of σ is shown in Figure 5. As expected, no strong variations of conductivity are found with respect to the obtained ‘wideband’ value of $\sigma = 3400$ S/m. Nevertheless, the obtained results could guarantee higher accuracy in simulations related to the design of antennas and microwave circuits at specific frequencies.

3 | FULLY 3D-PRINTED ANTENNAS FOR ELECTRIFI CONDUCTIVITY VALIDATION

To validate the Electrifi electrical conductivity characterisation, three fully 3D-printed monopole antennas, working on different sub-6 GHz bands, have been designed on 15×15 cm² ground planes and then fabricated and measured. Then, their performance has been compared with some copper-made twins, used as reference.

First, two bow-tie-like monopole antennas have been designed to operate at 2.8 and 4 GHz, respectively. The layout adopted for the monopole element is reported in Figure 6a with related parameters and size. In particular, starting from a standard bow-tie monopole, some lateral slots have been etched along the antenna’s edge to increase the current path, thus lowering the antenna’s electrical size. The electrical conductivity

value that minimised the RMSE in the appropriate frequency window (Table 2) has been set in the CST Microwave Studio® environment to perform specific simulations. Then, a third antenna, operating in an ultrawide band (i.e. 1.3–7.5 GHz) and covering almost the whole characterisation range, has been simulated by exploiting the design proposed by Stutzman et al. in Ref. [38] (Stutzman's antenna hereafter) and depicted in Figure 6b with related parameters and size. In this case, the value

of electrical conductivity that minimise the RMSE over the whole operational bandwidth, which is equal to 3400 S/m, has been set in the electromagnetic software to suitably model the antenna. Both radiating elements and ground planes have been manufactured by laying down a 0.4 mm-thick conductive layer of Electrifi on a 0.8 mm-thick substrate of PLA to make all the antennas mechanically robust. In this way, stiffer prototypes of fully 3D-printed antennas can be fabricated, and sufficiently rigid PLA substrates can be used to apply the adhesive copper tape of the twin antennas. The used printing settings are listed in Table 1.

Once printed, the Electrifi radiating elements have been properly connectorised by using female SMA connectors applied with two-component silver conductive glue by MG Chemicals [46]. On the other hand, the copper-made twin antennas have been realised using an adhesive copper tape shaped using a Graphtec CE6000 Cutting plotter, according to the technique proposed in Ref. [47], and then attached on the PLA substrate. In Figure 7a the copper and Electrifi versions

TABLE 2 RMSE and corresponding electrical conductivity for different frequency bands

Band [GHz]	RMSE [dB]	σ [S/m]
0.72–2.5	0.84	2500
2.0–3.5	0.32	2800
3.0–4.5	0.25	3100
4.0–6.0	0.35	3650

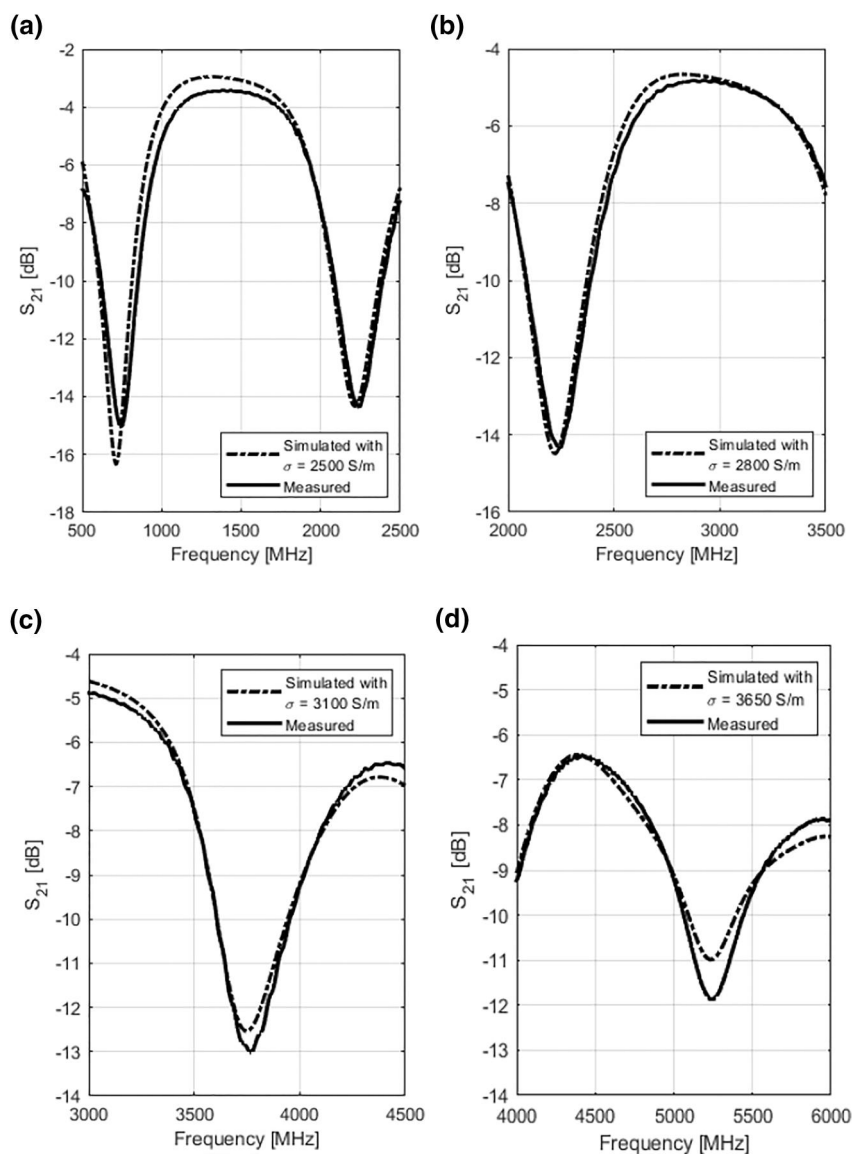


FIGURE 5 Comparison among the measured S_{21} target curve (solid line) and the simulated one (dotted line) with the value of electrical conductivity that minimised the root mean square error (RMSE), respectively, between (a) 0.5–2.5 GHz, (b) 2–3.5 GHz, (c) 3.0–4.5 GHz, and (d) 4.0–6.0 GHz

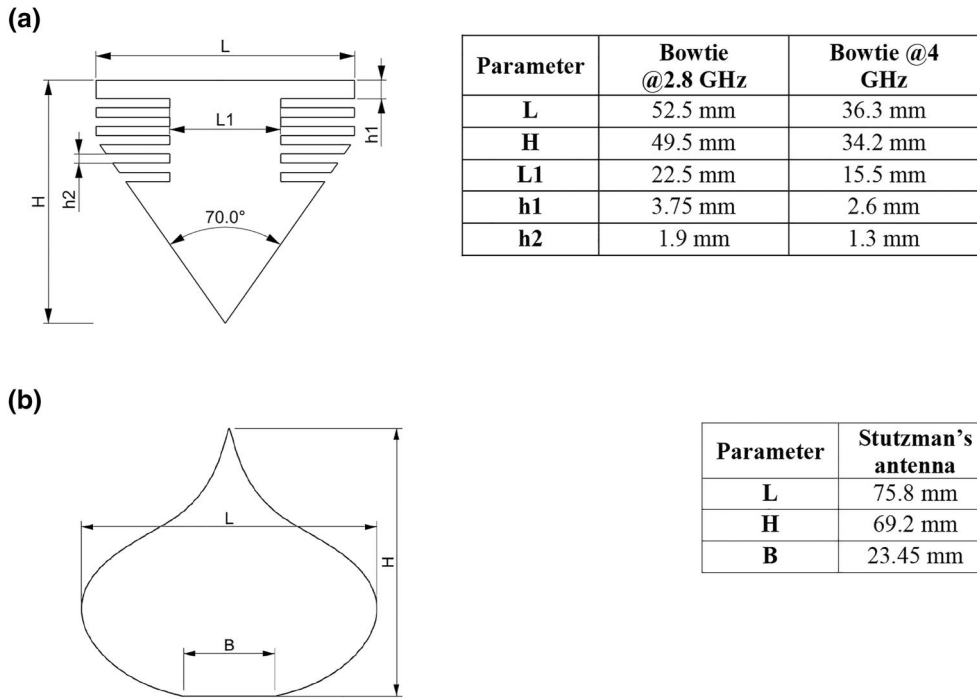


FIGURE 6 Layout and geometrical parameters values of the radiating elements considered in this paper: (a) the bow-tie antenna for both the 2.8 and 4 GHz resonance frequency and (b) the ultrawideband Stutzman's antenna [38]

of the three radiating elements are shown. In Figure 7b, a detail of the Stutzman's antenna in the two different versions is shown when mounted on the ground plane.

The reflection coefficient of the realised prototypes (AUTs), their far-field radiation pattern and gain have been measured in an anechoic chamber by exploiting the measurement setup depicted in Figure 7c by using the Anritsu MS46322 B two-port VNA and a calibrated antenna (model HyperLOG 7060 by AARONIA AG).

Specifically, the gain of the AUTs has been measured by exploiting the Friis transmission formula [48].

$$\frac{P_R}{P_T} = G_T G_R \left(\frac{\lambda}{4\pi R} \right)^2 \tag{1}$$

wherein

- P_R is the power available at the receiving antenna, which is the AUT with gain G_R ;
- P_T is the power available at the transmitting antenna, that is, the HyperLOG 7060, with known calibrated gain G_T ;
- R is the separation of the antennas;
- λ is the free space wavelength.

The ratio in Equation (1) is equal to the square amplitude of the transmission coefficient, which is measured using the two-port VNA, thus providing the measured gain of the AUT.

The HyperLOG 7060 antenna has been connected to a broadband low noise pre-amplifier (LNA) (model ZX60-83LN-S+ by Minicircuits) to improve the sensitivity of the

measurement. The LNA gain has been accurately measured using the VNA to obtain a reliable estimation of the AUTs-gain.

Measured and simulated reflection coefficients of the six antennas are reported in Figure 8 and organised to facilitate the mutual comparison. In particular, Figure 8a,b refers to the copper and Electrifi versions of the 2.8 GHz monopole antenna, respectively; Figure 8c,d refers to the copper and Electrifi versions of the 4.0 GHz monopole antenna, respectively; and Figure 8e,f refers to the copper and Electrifi versions of the ultrawideband Stutzman's antenna, respectively. It can be observed that there is a good agreement between the simulated and measured reflection coefficients of the six antennas. Despite negligible differences between the simulated and measured curves, likely due to fabrication and connectorisation processes, the comparison between the simulated and measured curves for the Electrifi antenna versions demonstrate that the estimated values of dielectric permittivity and electrical conductivity reported in Table 2 are suitable to design an accurate numerical model. Moreover, by considering the presence of comparable resonance frequency peaks in both the Electrifi and the copper-twin reference antenna, it is possible to assess that the above measured conductive characteristics of the Electrifi filament are suitable to design fully 3D-printed antennas and RF circuits.

To confirm this outcome, the radiative characteristics of the six antennas have been also investigated in terms of radiation pattern and gain. In Figure 9 the simulated and measured radiation patterns of each antenna are plotted on the E-plane. Only the upper hemisphere on top of the ground plane has been measured because of the inaccuracy of the measure for

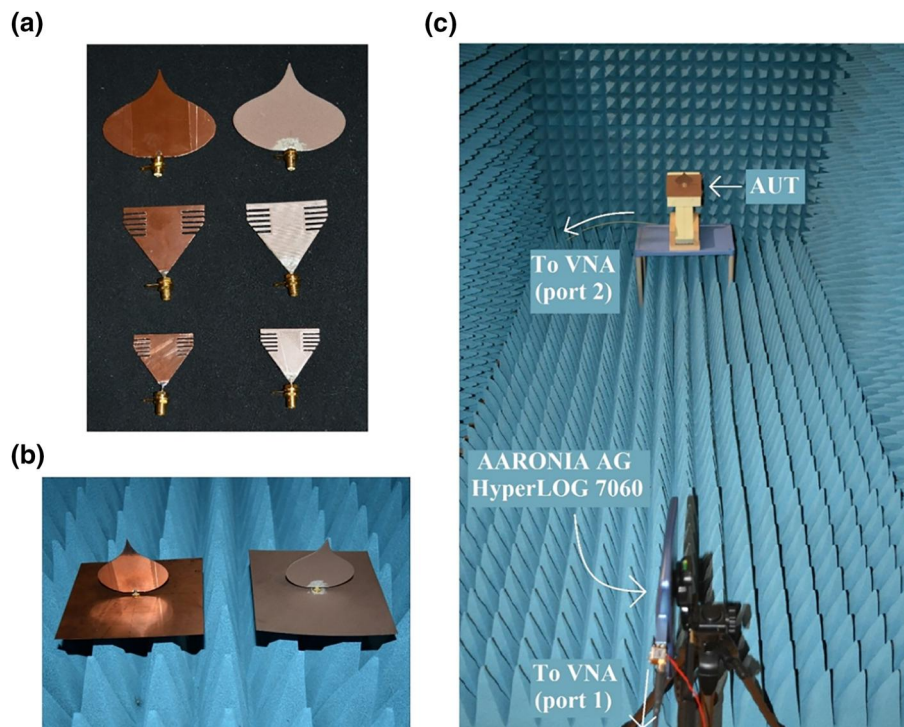


FIGURE 7 Prototypes of the realised antennas (a) and (b) (left: copper antennas; right: 3D-printed antennas) and measurement setup in an anechoic chamber: the AUT in the photo is the prototype of the fully 3D-printed Stutzman's antenna (c)

the lower hemisphere, due to the presence of the cable and connector. Specifically, Figure 9a,b refers to the copper and Electrifi versions of the 2.8 GHz monopole antenna, respectively, and the radiation patterns are obtained at the resonance frequency. Figure 9c,d refers to the copper and Electrifi versions of the 4.0 GHz monopole antenna, respectively, and the radiation patterns are obtained at the resonance frequency. Figure 9e,f refers to the copper and Electrifi versions of the ultrawideband Stutzman's antenna, respectively, and the radiation patterns are obtained at the frequency of 2 GHz. Finally, Figure 9g,h refers to the copper and Electrifi versions of the ultrawideband Stutzman's antenna, respectively, and the radiation patterns are obtained at the frequency of 6 GHz.

The numerical and measured normalised radiation patterns are almost overlapped for all the considered antennas. It is worth noting also that the normalised measured radiation pattern of the Electrifi and copper versions are comparable for all the antennas, even at higher frequencies (e.g. 6 GHz). Simulated and measured maximum gain values are listed in Table 3 at different frequencies and for all the antenna versions, including (in bold) the difference between simulated gain of copper and Electrifi versions, and the difference between measured gain of copper and Electrifi versions. As expected, the gain of the Electrifi antennas is generally lower than the gain of the copper twin antennas, due to the lower conductivity. Specifically, the difference between the simulated gain of the copper antennas and the Electrifi antennas averaged over the frequency band is as low as 0.4 dB. Similarly, the average difference between the measured gain of the copper antennas and the Electrifi antennas is as low as 0.58 dB. Finally, it is

worth noting that the difference between the simulated and measured maximum gain of the Electrifi antennas is generally lower than 0.5 dB.

These outcomes demonstrate once again the effectiveness of the performed Electrifi and PLA material characterisation with particular reference to the suitability of the Electrifi filament in the antenna and RF circuit design, with the tangible advantages of an easier prototyping process provided by the 3D printing technology.

4 | CONCLUSIONS

The desired massive exploitation of 3D-printing in electromagnetics for the realisation of both prototypes and, in prospective, final devices strictly depends on the designer's capability to rigorously simulate the electromagnetic properties of the extruded materials, including the conductive ones. In this work, an electromagnetic characterisation of a 3D-Printed conductive material in a rather wide band (i.e. 0.72–6 GHz) has been performed. The conductivity of one of the most promising conductive filaments, named Electrifi, has been experimentally evaluated and rigorously validated by designing three antennas operating at different frequencies, both in wide and ultrawide sub-6 GHz bands. All the Electrifi antennas have been designed and then prototyped by considering the related copper-made twins, used as reference. Results in terms of reflection coefficient, radiation pattern and gain have been obtained and compared. The good agreement between simulated and measured results, as well as the good matching

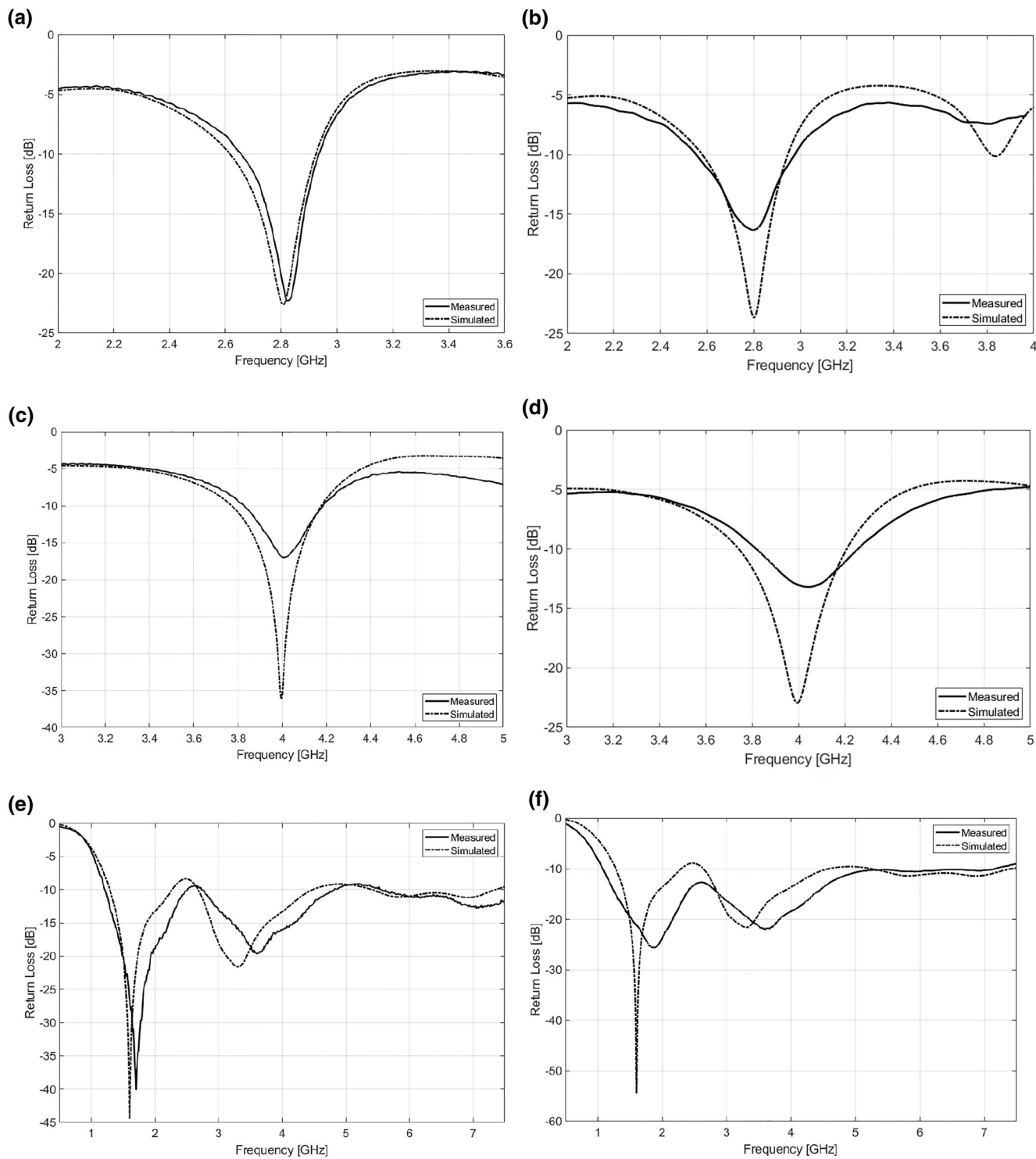


FIGURE 8 Comparison between the measured and simulated reflection coefficient, respectively, for: (a) copper and (b) Electrifi version @2.8 GHz; (c) copper and (d) Electrifi version @4.0 GHz; (e) copper and (f) Electrifi ultrawideband Stutzman's antenna

between the Electrifi and copper antenna performance, demonstrate the effectiveness of the presented characterisation of the Electrifi conductivity for designing and printing effectively working electromagnetic devices up to 6 GHz.

ACKNOWLEDGEMENT

This work has been partially supported by Fondazione di Sardegna under project “SISCO—ITC methodologies for the security of complex systems”, CUP: F74I19001060007.

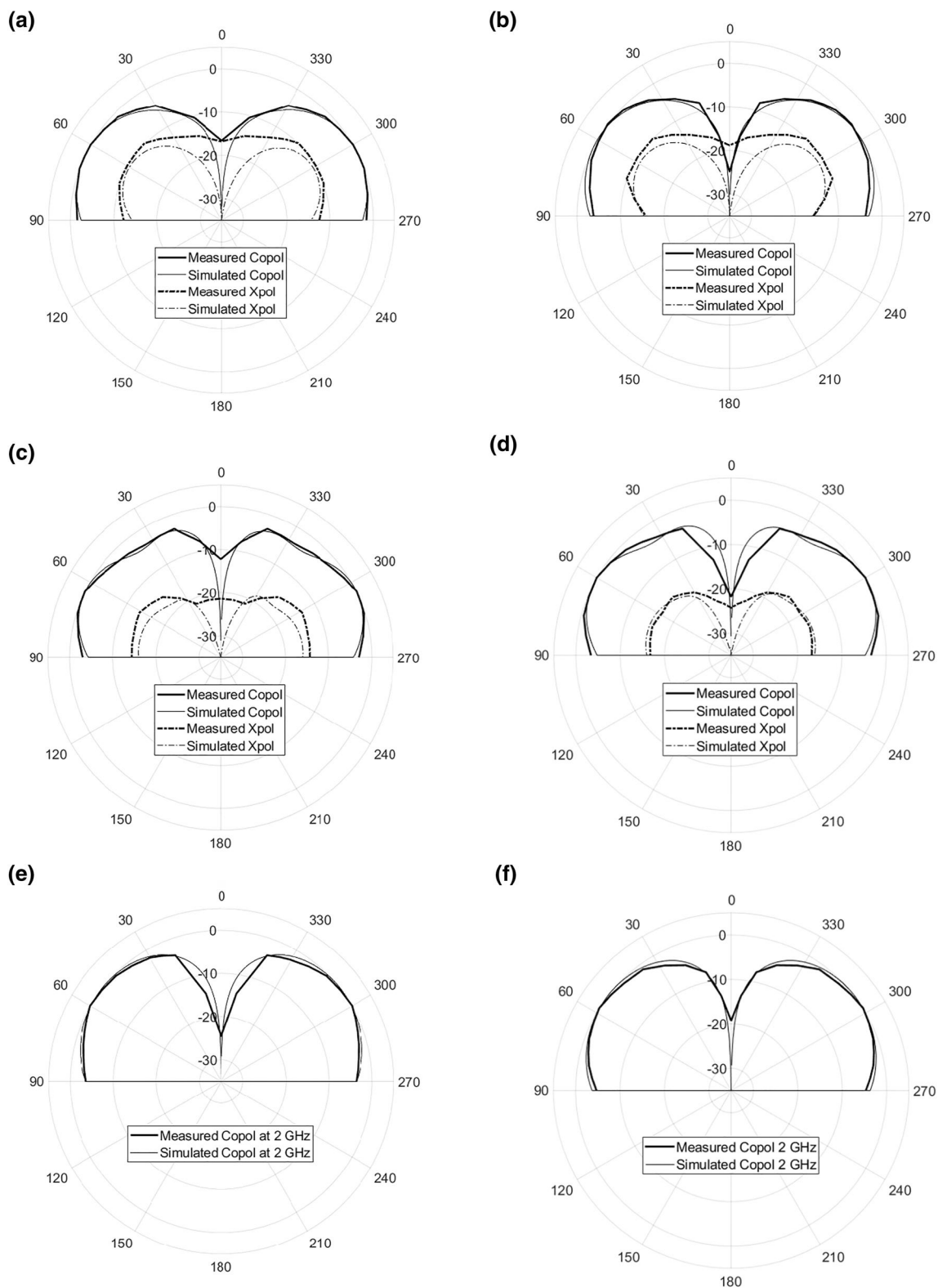


FIGURE 9 Comparison between normalised measured and simulated radiation patterns for: (a) copper and (b) Electrifi version @2.8 GHz; (c) copper and (d) Electrifi version @4.0 GHz; (e) copper and (f) Electrifi version of the Stutzman's antenna @2 GHz; (g) copper and (h) Electrifi version of the Stutzman's antenna @6 GHz

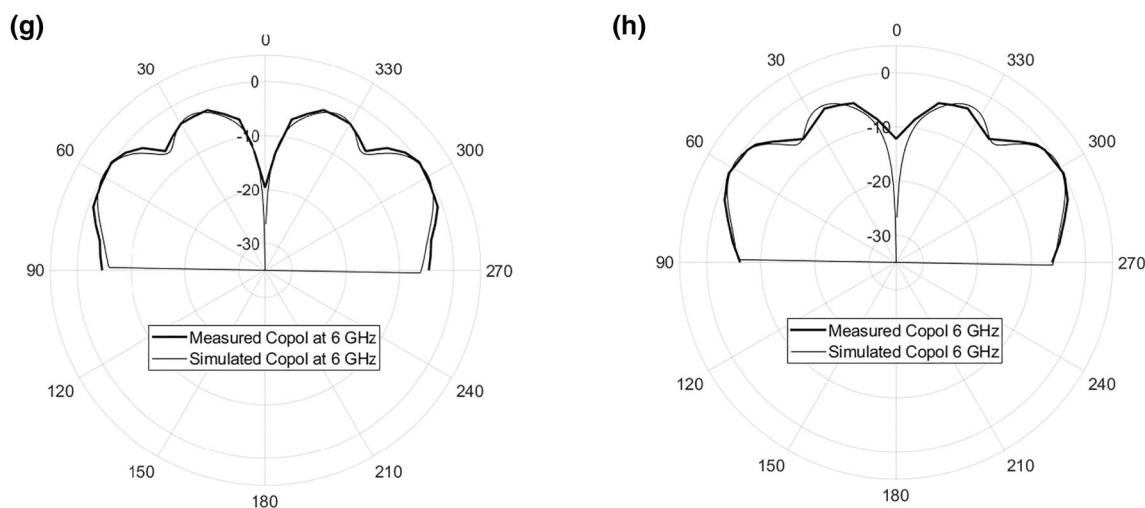


FIGURE 9 (Continued)

TABLE 3 Simulated and measured gain for all the realised antenna prototypes

	Stutzman's antenna [38]					Bowtie @2.8 GHz	Bowtie @4.0 GHz
Frequency [GHz]	2.00	3.00	4.00	5.00	6.00	2.80	4.00
Simulated gain [dBi] (Copper)	4.27	6.81	5.22	5.17	6.12	3.83	4.36
Simulated gain [dBi] (Electrifi)	4.00	6.52	4.90	4.87	5.81	3.15	3.71
Simulated gain difference [dB]	-0.27	-0.29	-0.32	-0.30	-0.31	-0.68	-0.65
Measured gain [dBi] (Copper)	4.4	6.6	5.3	5.1	6.3	4.0	4.1
Measured gain [dBi] (Electrifi)	3.9	6.0	4.7	4.7	5.8	3.2	3.5
Measured gain difference [dB]	-0.5	-0.6	-0.6	-0.4	-0.5	-0.8	-0.6

CONFLICT OF INTEREST

The author declares that there is no conflict of interest that could be perceived as prejudicing the impartiality of the research reported.

PERMISSION TO REPRODUCE MATERIALS FROM OTHER SOURCES

None.

DATA AVAILABILITY STATEMENT

The data that support the findings of this study are available from the corresponding author upon reasonable request.

ORCID

Andrea Michel  <https://orcid.org/0000-0001-8074-113X>

Luca Catarinucci  <https://orcid.org/0000-0001-9735-6844>

REFERENCES

- Johnson, K., et al.: Digital manufacturing of pathologically-complex 3D printed antennas. *IEEE Access* 7, 39378–39389 (2019). <https://doi.org/10.1109/access.2019.2906868>
- Colella, R., et al.: Fully 3D-printed RFID tags based on printable metallic filament: performance comparison with other fabrication techniques. In: 2019 IEEE-APS Topical Conference on Antennas and Propagation in Wireless Communication (APWC), pp. 253–257. Granada (2019)
- Rojas-Nastrucci, E.A., et al.: Ka-band characterization of binder jetting for 3-D printing of metallic rectangular waveguide circuits and antennas. In: *IEEE Transactions on Microwave Theory and Techniques* 65(9), pp. 3099–3108 (2017)
- Colella, R., Michel, A., Catarinucci, L.: Compact 3-D-printed circularly polarized antenna for handheld UHF RFID readers. *IEEE Antenn. Wireless Propag. Lett.* 17(11), 2021–2025 (2018). <https://doi.org/10.1109/lawp.2018.2860253>
- Mirmozafari, M., et al.: Direct 3-D printing of nonplanar linear-dipole-phased array antennas. *IEEE Antenn. Wireless Propag. Lett.* 17(11), 2137–2140 (2018)
- Nassar, I.T., Weller, T.M., Tsang, H.: A 3-D printed miniaturized log-periodic dipole antenna. In: *IEEE Antennas and Propagation Society International Symposium*, pp. 6–11. Memphis (2014)
- Smith, K., Adams, R.: A broadband 3D printed fractal tree monopole antenna. *Prog. In Electromagn. Res. C* 86, 17–28 (2018). <https://doi.org/10.2528/pierc18030505>
- Farooqui, M.F., Kishk, A.: 3-D-Printed tunable circularly polarized microstrip patch antenna. *IEEE Antenn. Wireless Propag. Lett.* 18(7), 1429–1432 (2019)
- Adeyeye, A.O., Bahr, R.A., Tentzeris, M.M.: 3D printed 2.45 GHz yagi-uda loop antenna utilizing microfluidic channels and liquid metal. In: 2019 IEEE International Symposium on Antennas and Propagation and USNC-URSI Radio Science Meeting, pp. 1983–1984. Atlanta (2019)
- Wang, S., Zhu, L., Wu, W.: 3-D printed inhomogeneous substrate and superstrate for application in dual-band and dual-CP stacked patch antenna. *IEEE Trans. Antenn. Propag.* 66(5), 2236–2244 (2018)

11. Bahr, R.A., et al.: Novel uniquely 3D printed intricate voronoi and fractal 3d antennas. In: 2017 IEEE MTT-S International Microwave Symposium (IMS), pp. 1583–1586. Honolulu (2017)
12. Ghazali, M.I.M., Chahal, P.: A 3D printed cavity backed 2x4 slotted waveguide antenna array. In: 2018 IEEE International Symposium on Antennas and Propagation & USNC/URSI National Radio Science Meeting, pp. 1435–1436. Boston (2018)
13. Teniente, J., et al.: 3-D printed horn antennas and components performance for space and telecommunications. *IEEE Antenn. Wireless Propag. Lett.* 17(11), 2070–2074 (2018)
14. Bongard, F., et al.: 3Dprinted Ka-band waveguide array antenna for mobile SATCOM applications. In: 2017 11th European Conference on Antennas and Propagation (EUCAP), pp. 579–583. Paris (2017)
15. Bjorgaard, J., et al.: Design and fabrication of antennas using 3D printing. *Prog. In Electromagn. Res. C* 84, 119–134 (2018). <https://doi.org/10.2528/pierc18011013>
16. Gu, C., et al.: A D-band 3D-printed antenna. In: *IEEE Transactions on Terahertz Science and Technology* (2020)
17. Martínez Odiaga, H.J., Yarlequé Medina, M.A., Navarro, S.A.: An implemented 3D printed circular waveguide antenna for K band Applications. In: *IEEE MTT-S Latin America Microwave Conference (LAMC 2018)*, pp. 1–3. Arequipa (2018)
18. Alkaraki, S., et al.: Compact and low-cost 3-D printed antennas metalized using spray-coating technology for 5G mm-wave communication systems. *IEEE Antenn. Wireless Propag. Lett.* 17(11), 2051–2055 (2018)
19. Alkaraki, S., et al.: 3D printed corrugated plate Antennas with high aperture efficiency and high gain at X-band and ka-band. *IEEE Access* 8, 30643–30654 (2020). <https://doi.org/10.1109/access.2020.2972101>
20. Lomakin, K., et al.: 3D printed slotted waveguide array antenna for automotive radar applications in W-band. In: 15th European Radar Conference (EuRAD), pp. 389–392. Madrid (2018)
21. Gjakaj, V., et al.: A novel 3D printed half-width microstrip leaky-wave antenna. In: 2017 IEEE International Symposium on Antennas and Propagation & USNC/URSI National Radio Science Meeting, pp. 1249–1250. San Diego (2017)
22. Castro, A.T., Sharma, S.K.: A triple mode waveguide corrugated horn antenna using 3D printing technology. In: 2017 IEEE International Symposium on Antennas and Propagation & USNC/URSI National Radio Science Meeting, pp. 1235–1236. San Diego (2017)
23. Kotzé, K., Gilmore, J.: SLM 3D-printed horn antenna for satellite communications at X-band. In: 2019 IEEE-APS Topical Conference on Antennas and Propagation in Wireless Communication (APWC), pp. 148–153. Granada (2019)
24. Lomakin, K., et al.: Evaluation and characterization of 3-D printed pyramid horn antennas utilizing different deposition techniques for conductive material. In: *IEEE Transactions on Components, Packaging and Manufacturing Technology*, vol. 8(11), pp. 1998–2006 (2018)
25. Helena, D., et al.: Antenna design using modern additive manufacturing technology: a review. *IEEE Access* 8, 177064–177083 (2020). <https://doi.org/10.1109/access.2020.3027383>
26. Luo, N., et al.: Experimental verification of 3D metal printed dual circular-polarized horn antenna at V-band. In: 2019 Antenna Measurement Techniques Association Symposium (AMTA), pp. 1–6. San Diego (2019)
27. Decrossas, E., et al.: Evaluation of 3D printing technology for corrugated horn antenna manufacturing. In: 2016 IEEE International Symposium on Electromagnetic Compatibility (EMC), pp. 251–255. Ottawa (2016)
28. Fiberforce Website [Online]. <http://www.fiberforce.it/products-pro>. Accessed 01 Aug 2021
29. Proto-pasta Website [Online]. <https://www.proto-pasta.com/pages/conductive-pla>. Accessed 01 Aug 2021
30. BlackMagic3D Website [Online]. <http://www.blackmagic3d.com/Conductive-p/grphn-pla.htm>. Accessed 01 Aug 2021
31. Multi3D Website [Online]. <https://www.multi3dllc.com>. Accessed 01 Aug 2021
32. Roy, S., et al.: A model for 3D-printed microstrip transmission lines using conductive electrifi filament. In: *IEEE International Symposium on Antennas and Propagation & USNC/URSI National Radio Science Meeting*, pp. 1099–1100. San Diego (2017)
33. Mitra, D., et al.: On the design of an improved model of additively manufactured microstrip transmission lines for radio frequency applications. In: 2019 IEEE International Conference on Electro Information Technology (EIT), pp. 182–184. Brookings (2019)
34. Pizarro, F., et al.: Parametric study of 3D additive printing parameters using conductive filaments on microwave topologies. *IEEE Access* 7, 106814–106823 (2019). <https://doi.org/10.1109/access.2019.2932912>
35. Mitra, D., et al.: Conductive electrifi and nonconductive NinjaFlex filaments based flexible microstrip antenna for changing conformal surface applications. *Electronics* 10(7), 821 (2021). <https://doi.org/10.3390/electronics10070821>
36. Salazar, R., et al.: Assessment of 3D-printed waveguides using conductive filaments and a chloroform-based smoothing process. *Addit. Manuf.* 51, 102593 (2022). <https://doi.org/10.1016/j.addma.2022.102593>
37. García-Martínez, H., et al.: Low-cost additive manufacturing techniques applied to the design of planar microwave circuits by fused deposition modeling. *Polymers* 12(9), 1946 (2020). <https://doi.org/10.3390/polym12091946>
38. Suh, S.-Y., Stutzman, W.L., Davis, W.A.: A new ultrawideband printed monopole antenna: the planar inverted cone antenna (PICA). *IEEE Trans. Antenn. Propag.* 52(5), 1361–1364 (2004)
39. Honari, M.M., et al.: Investigation of the 3D printing roughness effect on the performance of a dielectric rod antenna. *IEEE Antenn. Wireless Propag. Lett.* 17(11), 2075–2079 (2018)
40. Shamvedi, D., et al.: Improved performance of 3D metal printed antenna through gradual reduction in surface roughness. In: 2017 International Conference on Electromagnetics in Advanced Applications (ICEAA), pp. 669–672. Verona (2017)
41. Hawatmeh, D.F., et al.: Embedded 6-GHz 3-D printed half-wave dipole antenna. *IEEE Antenn. Wireless Propag. Lett.* 16, 145–148 (2017). <https://doi.org/10.1109/lawp.2016.2561918>
42. Lähti, K., et al.: A review of microstrip T-resonator method in determining the dielectric properties of printed circuit board materials. *IEEE Trans. Instrum. Meas.* 56(5), 1845–1850 (2007)
43. Catarinucci, L., et al.: Microwave characterisation of polylactic acid for 3D-printed dielectrically controlled substrates. *IET Microw., Antennas Propag.* 11(14), 1970–1976 (2017)
44. Boussatour, G., et al.: Dielectric characterization of polylactic acid substrate in the frequency band 0.5–67 GHz. *IEEE Microw. Wireless Compon. Lett.* 28(5), 374–376 (2018)
45. CST Website [Online]. <http://www.cst.com>. Accessed 01 Aug 2021
46. MG Chemicals 8331 Conductive Glue [Online]. <https://www.mgchemicals.com/products/adhesives/electrically-conductive-adhesives/silver-conductive-epoxy>. Accessed 10 Jan 2022
47. Catarinucci, L., Colella, R., Tarricone, L.: Smart prototyping techniques for UHF RFID tags: electromagnetic characterization and comparison with traditional approaches. *Electromagn. Waves* 132, 91–111 (2012). <https://doi.org/10.2528/pier12080708>
48. IEEE recommended practice for antenna measurements, *IEEE Std 149-2021 (Revision of IEEE Std 149-1977)*, pp.1–207, (2022)

How to cite this article: Colella, R., et al.: Electromagnetic characterisation of conductive 3D-Printable filaments for designing fully 3D-Printed antennas. *IET Microw. Antennas Propag.* 16(11), 687–698 (2022). <https://doi.org/10.1049/mia2.12278>